IEEE Access
Multidisciplinary | Rapid Review | Open Access Journal

Received January 5, 2021, accepted January 15, 2021, date of publication January 19, 2021, date of current version November 15, 2021.

Digital Object Identifier 10.1109/ACCESS.2021.3052777

Performance of a Twin-Intake Diesel Engine With Guide Vanes During an Intake Stroke Revealed Through Simulations and Experiments

HAILIN KUI[1], YUNZHEN GUO[1], CHANGRAN FU[2], AND SHENGWEI PENG[1]
[1]College of Transportation, Jilin University, Changchun 130022, China
[2]China National Heavy Duty Truck Group Co., Ltd., Jinan 250101, China

Corresponding author: Yunzhen Guo (guoyz18@mails.jlu.edu.cn)

This work was supported by the National Natural Science Foundation of China 51776086.

ABSTRACT To improve the flow characteristics of diesel engines with twin intake ports, this study evaluates the installation of guide vanes of varying lengths, heights and angles in front of the intake runner of a CA4DD diesel engine. Considering the interference among various parameters of the guide vane, the parameters were studied with uniform design. To study the effect of guide vanes on the twin-intake diesel engine during the intake stroke, 9 guide vane models, where the vane lengths were 30-70 mm, the vane heights were 1.5-13.5 mm, and the vane angles were 4-36°, were compared with a base model without a guide vane. CATIA was used to build a simulation model, and XFLOW was used to run a three-dimensional (3D) computational fluid dynamics (CFD) simulation. Simulation of different valve lifts of 2-10 mm in steps of 2 mm showed that the guide vane slightly affected the flow coefficient and obviously affected the swirl ratio. Furthermore, designs 4, 5 and 6 had different performance improvements under different valve lifts. The velocity and vorticity of the in-cylinder were evaluated. Moreover, 9 guide vane models were fabricated and tested on a steady-flow test bench. The experimental results show that the swirl ratio average increase of the guide vane models compared to the base model is 21%. The maximum increase is 39% when the guide vane height is 6 mm, the length is 65 mm, and the angle is 24°; when the guide vane height is 7.5 mm, the length is 50 mm, and the angle is 20°, the average increase is 27%. The flow coefficient is less affected and fluctuates at approximately 2%. Hence, the experiments and simulations in this work yield consistent results, and the application of guide vane models compared to a base model can improve the performance of diesel engines.

INDEX TERMS Computational fluid dynamics, flow characteristics, guide vane, steady-flow test.

I. INTRODUCTION

Stringent environmental regulations and fuel economy standards are a part of technological progress [1]. With increasingly stringent emission requirements, emission targets will be the most challenging task in the near future [2]. Most small and medium-sized high-speed diesel engines use semi-open combustion chambers, which require strong intake swirls [3]. The intake port plays a very important role in the diesel engine intake system [4], [5]. Two parameters are important to evaluate the flow characteristics of diesel engines: flow coefficient and swirl ratio. The flow coefficient describes the intake capacity of a diesel engine. The swirl ratio greatly affects the fuel air mixing, premixed combustion, diffusion combustion and combustion stability of diesel engines [6]. However, the swirl organization in a diesel cylinder mainly depends on the shape of the intake port, and there is a contradictory effect between flow coefficient and swirl ratio. Therefore, it is very difficult to simultaneously improve both parameters [7]. Generally, the flow characteristics of diesel engines are improved by increasing one of these two parameters while the other remains constant or slightly decreases.

The intake swirl directly affects the mixture of oil and gas, combustion, power, economic performance and emissions of the engine [8]. In recent years, related research on improving the swirl ratio of diesel engines has been performed by

The associate editor coordinating the review of this manuscript and approving it for publication was Wen Chen.

researchers in various countries. Du and Li [9] studied how the parameters of guide vanes in swirlers for diesel engines affected the air flow between the vanes. Xin *et al.* [10] developed a new variable, i.e., the swirl intake manifold, for a 4-valve direct-injection diesel engine by installing a swirl control valve in the intake manifold. Bari *et al.* separately investigated the effect of guide vanes with different angles [11], [12], lengths [13], and heights [14], [15] and in different numbers [16], [17], which were installed in front of the intake runner, on the performance of a compression ignition (CI) engine [18]. The authors found that guide vane models could improve the performance of and reduce emissions from compression ignition engines. In general, a guide vane has 4 main parameters: vane angle, vane length, vane height and vane number. To produce a guide vane with the best design, all parameters must be optimized.

However, previous studies evaluated the effect of only a single parameter on the diesel engine performance, while the other parameters remained unchanged. The mutual interference among the parameters of the guide vanes is very important. Interferences among different parameters will impact the resulting engine performance, but it is difficult to directly study the interference among various parameters of the guide vane in the intake. Therefore, a test bench with CFD simulation for study. The CFD simulation can show the distribution of various flow fields in the cylinder, which cannot be achieved in bench tests. Many scholars use CFD to analyze the intake flow characteristics to design and investigate the intake port [19]–[21].

This study overcomes the shortcomings of previous studies. Consider the mutual interference among various parameters, we mainly focus on multiple guide vane parameters, which can be varied together to enhance the performance of a diesel engine by analyzing the flow characteristics of the intake and flow field distribution in the cylinder. Therefore, the vane length, vane height and vane angle were optimized, while the vane number remained fixed in this study. The guide vane parameters were determined by a uniform design method. The flow field of the guide vane models was analyzed by CFD simulation. Then, a steady-flow test bench with a twin-intake diesel engine was run with the vanes installed in front of the intake port. The effect of the guide vanes on the swirl ratio and flow coefficient was analyzed. This study combines the simulation and experimental results. The flow characteristics without and with guide vanes were compared to explore the effect of these designs. Finally, the effects of different designs on different valve lifts are studied, and the guide vane parameters with the best comprehensive effect are determined, which provides a theoretical reference to improve the performance of the diesel engine. The details of these processes are described in the following section.

II. TEST DESIGN

A. TEST PROCESS

In this article, the test design is based on a uniform design to study the effect of the guide vanes on the performance of dual inlet diesel engine during the intake. The overall process is shown in Fig. 1. First, to increase the swirl of the twin-intake diesel engine, the parameters of the guide vane are determined by the uniform design. Then, the guide vane models are established to conduct the CFD simulation and steady-flow test. Finally, by analyzing the effect of the guide vane on the flow characteristics of the twin-intake diesel engine, the optimal guide vane parameters were determined.

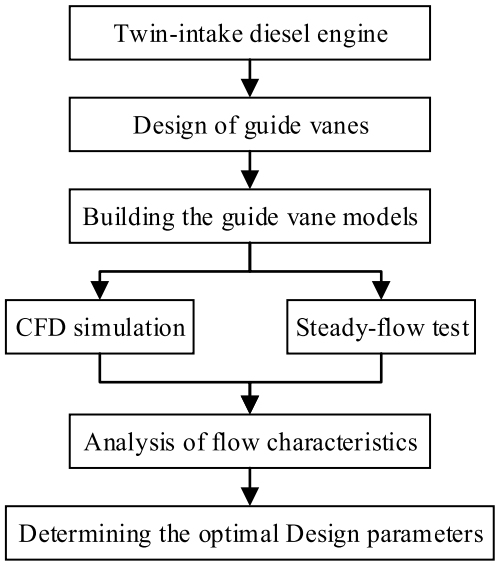

FIGURE 1. Flowchart of the overall process.

B. DESIGN OF GUIDE VANE

Several factors were considered in the guide vane design. In theory, a larger vane angle obstructs the airflow more. Furthermore, the surface area of the guide vane depends on the vane length and vane height, which are positively correlated with the swirl ratio and negatively correlated with the flow coefficient. In this study, the uniform design method was used to determine the guide vane parameters. The uniform design method is an experimental design method, where a group of points is sampled from a given set of points to uniformly scatter the sampled points [22]. The sampled point values obtained with the uniform design evenly scatter and do not depend on one another [23], [24]. The uniform design method ensures that all available information is obtained, and the number of required experiments is minimized [25]. If there are n factors and q levels, q^n pairs of different values can be found. We can select q pairs of values that can evenly scatter over the q^n pairs of values by the uniform design method. Lu *et al.* used the uniform design to obtain test points and response surface, which were used in the design of a turbofan engine [26]. He *et al.* studied the comprehensive evaluation of the sound quality by a uniform design method, which can accurately provide the ranks of sound stimulation [27]. The number of levels is more than twice the number of factors to satisfy the uniform design criteria. In this study, the number of factors was 3, and the levels per factor were 9.

TABLE 1. Uniform design scheme.

Design Number	Height (mm)	Length (mm)	Angle (°)
1	1.5	60	36
2	3.0	45	32
3	4.5	30	28
4	6.0	65	24
5	7.5	50	20
6	9.0	35	16
7	10.5	70	12
8	12	55	8
9	13.5	40	4

Therefore, the uniform design table $U_9^*(9^4)$ was selected. More details about the uniform design method are shown in the literature [28]–[30].

Considering the shape of the intake port, the number of guide vanes was determined to be 4, which were arranged at 90° to each other in front of the helical intake port. Therefore, there were 3 variable parameters of the guide vane in this study: vane length (H), vane height (L) and vane angle (θ). Referring to Du and Li [9], Xin *et al.* [10], and Bari and Saad [11]–[16], this article determined the value range of the three factors. According to the actual size, the vane height was 1.5-13.5 mm with steps of 1.5 mm, the vane length was 30-70 mm with steps of 5 mm, and the angle was 4-36° with steps of 4°. There were 9 levels per factor. According to the uniform design use table, the uniform design scheme of this study was determined, as shown in Table 1. There were 9 sets of designs with different heights, lengths and angles. We numbered these designs from 1 to 9. For identification purposes, the names of different guide vane designs were composed of the height, length and angle; for example, H1.5-L60-θ36 indicates a height of 1.5 mm, a length of 60 mm and an angle of 36°, as shown in design number 1 of Table 1. Other designs were similarly named.

III. CFD SIMULATION

This study used CATIA to draw the simulation model under different valve lifts. The simulation model was imported into the CFD software in.STP format to simulate different designs with and without a guide vane. Ten simulation models were run, including 1 base model without a guide vane and 9 guide vane models with different guide vanes. There were 3 important processes in the simulation: drawing the simulation model, setting the boundary conditions and postprocessing the simulation data. The details of the simulation are explained in the next section.

A. SIMULATION MODEL

In this study, the base model for simulation was established according to a FAW-Dalian Diesel CA4DD diesel engine.

TABLE 2. Basic specifications of a CA4DD diesel engine.

Parameters	Details
Engine model	FAW-Dalian Diesel CA4DD
Stoke	104.9 mm
Bore	95.4 mm
Number of cylinder	4
Number of valve	4
Displacement	2.999 L
Intake diameter	29.6 mm
Length of connecting rod	162 mm

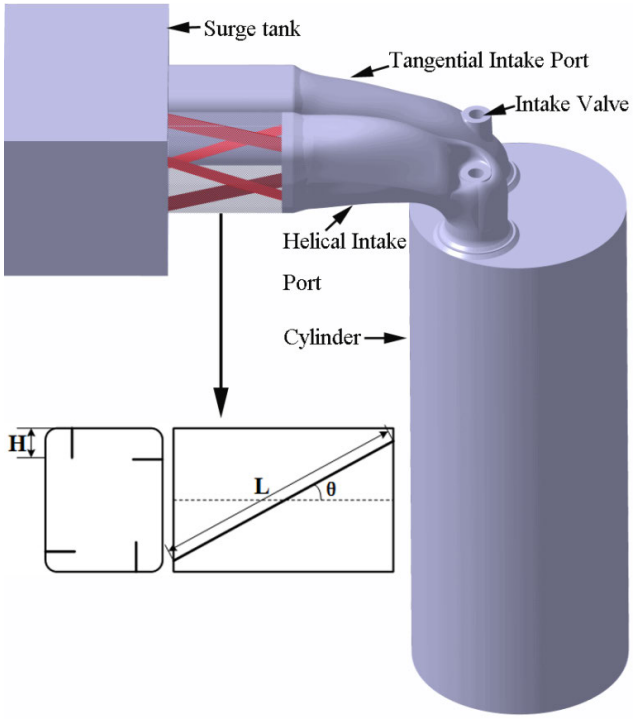

FIGURE 2. Guide vane model and the corresponding diagram.

A CA4DD diesel has two intake ports: a helical intake port and a tangential intake port. Different port combinations had different effects on the flow coefficient and swirl ratio [31]. The detailed basic specifications of a CA4DD diesel engine are provided in Table 2.

The guide vane model and corresponding diagram are shown in Fig. 2. According to the research in this field, the same assumption was made in this study as in previous studies. Nonuniformity between cylinders was ignored. It was assumed that the airflow between cylinders was evenly distributed, so that it could be simulated by one cylinder. Because of the intake process, assuming that the exhaust valve was closed, the exhaust valve and exhaust runner were omitted and replaced with a plane to reduce the computing domain of the model and computing time. By compromising

on these factors, the base simulation model has 4 main parts: a surge tank, a cylinder, an intake runner and an intake valve. The intake runner and intake valve of the base simulation model were drawn according to the actual diesel engine size to ensure that the simulation model was as close in shape to a real diesel engine as possible. The cylinders of the base simulation model were drawn in accordance with the actual dimensions and extended to 2.5 times the actual size to ensure the convergence of the model and reduce the backflow at the outlet. Since the helical intake port is mainly used to generate intake swirls, the guide vane was installed in front of the helical intake port of the base model.

B. SIMULATION SETTINGS

In XFLOW, a numerical study was performed for the intake process of twin intake ports in diesel engines, which is a unidirectional flow process, using the lattice-Boltzmann method (LBM). The LBM describes the motion of aerodynamic molecules through discretization and uses a regular grid to decompose the fluid domain into a set of lattice nodes. The fluid is modeled as a set of fluid particles that can move only between lattice nodes. The composition of the lattice nodes depends on the selected lattice model [32]. The lattice model for 3D simulations uses a cubic lattice with 15 discrete velocity directions [33]. The turbulence model adopts a large eddy simulation (LES) in a 3D spatial domain for different valve lifts. LES is a new numerical technique to study the transport of momentum and scalars under turbulence at high Reynolds numbers [34]. All turbulent structures larger than the filter scale are decomposed [35]. The governing equation of the LES model is generally obtained by filtering based on Navier-Stokes equations.

For simulation through XFLOW, step-independent and particle-independent analyses should be performed first. The details of the analysis and settings were described in previous studies [36]. The entire simulation model established in this study was set as a computational domain to calculate the fluid flow. Regional refinement with different accuracies was performed for regions with complex structures and small sizes to save computing resources and computing time. Three regions were refined: at the intake port, near the valve and at 1.75D (a distance 1.75 times the cylinder diameter from the top of cylinder). Fig. 3 shows the domain structure of the simulation model. This is a unidirectional flow process. The locations of the inlet and outlet are shown in Fig. 3. The pressure boundary condition was induced for the inlet and outlet. For the boundary condition, the pressure inlet is applied at the entry surface of the surge tank, and the pressure outlet is applied at the bottom surface of the cylinder. Other geometries are set as wall boundary conditions. The interior of the entire geometry is a fluid domain. The refinement algorithm uses adaptive refinement. Suppose that air is an ideal gas. The stability parameters tend to rapidly stabilize and be far less than 1. The detailed simulation boundary condition settings are shown in Table 3.

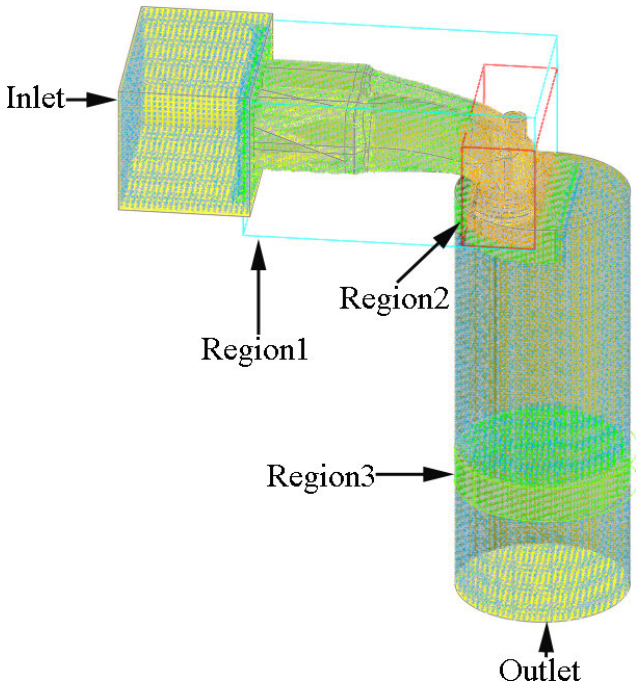

FIGURE 3. Domain structure of the simulation model.

TABLE 3. Boundary condition settings.

Boundary condition	Details
Inlet boundary condition	99350Pa
Outlet boundary condition	94350Pa
Refinement algorithm	adaptive refinement
Resolved scale	3 mm
Resolved scale of Region1	1.5 mm
Resolved scale of Region2	0.75 mm
Resolved scale of Region3	1.5 mm
Viscosity model	Newtonian
Dynamic viscosity	0.000017894 Pa • s
Operating temperature	288.15K

C. SIMULATION RESULTS

First, the flow characteristics of the base model with different valve lifts were investigated. Each model simulated 5 valve lifts: 2, 4, 6, 8, and 10 mm. Next, 9 guide vane models were studied: H1.5-L60-θ36, H3-L45-θ32, H4.5-L30-θ28, H6-L65-θ24, H7.5-L50-θ20, H9-L35-θ16, H10.5-L70-θ12, H12-L55-θ8, and H13.5-L40-θ4. Because the flow characteristics during the intake stroke affect the flame spreading velocity, combustion stability, and combustion efficiency, this article focuses on the region of the intake stroke. Investigations have shown that certain flow structures produced during the intake process persist through the compression stroke and enhance the air and fuel mixing near the top dead center [37].

The results of all 9 guide vane models were presented and compared to the base model with no guide vane. In addition, the in-cylinder flow field distributions of several models were analyzed. During the simulation, the swirl ratio was calculated by simulating the speed of the vane anemometer and engine. The dimensionless swirl is:

$$N_R = \frac{n_D}{n} \tag{1}$$

where n_D is the vane anemometer speed, and n is the engine speed.

In the simulation, the simulated speed of the vane anemometer was the rotation speed of a gas in rigid motion at the position of the vane anemometer in the experiment. Moreover, the vorticity is defined as the curl of the velocity and can be interpreted as twice the average angular velocity of a fluid element [38]. Thus, the simulated speed of the vane anemometer can be obtained. Furthermore, the axial velocity of gas in the simulated cylinder is used to replace the average speed of the piston. The engine speed can be obtained from the relationship between the average speed of the piston and the engine speed. The obtained engine speed is as follows:

$$n = \frac{30 \cdot m}{\rho \cdot \mathrm{A} \cdot \mathrm{S}} \tag{2}$$

where S is the piston stroke, A is the transverse-sectional area of the cylinder, and m is the inlet mass flow.

The flow coefficient is determined from (3):

$$C_f = \frac{m_{real}}{m_{th}} \tag{3}$$

where m_{real} is the real inlet mass flow, and m_{th} is the theoretical inlet mass flow. More details about C_f can be found in the literature [39].

In XFLOW, the real inlet mass flow can be directly output. The flow velocity multiplied by the transverse-sectional area yields the theoretical mass flow, which is determined by only the transverse-sectional area and differential pressure in the simulation. The absence of a vane anemometer in the simulation decreased the fluid resistance loss and slightly increased the swirl ratio, especially with a low valve lift. Below a valve lift of 2 mm, the swirl ratio greatly fluctuated and had poor comparability, as shown by both simulation and experiment. Thus, the flow characteristics with valve lifts of 4, 6, 8, and 10 mm were determined and compared.

As shown in Fig. 4, the simulated swirl ratio for different guide vane designs greatly fluctuated under the same valve lift, which illustrates that the guide vanes greatly affected the swirl ratio. There are two stages to simulate the swirl ratio and valve lift, and the 4-mm valve lift serves as a boundary point. The fluid resistance loss was lower in the simulation than in the steady-flow test. Therefore, the swirl ratio was slightly larger in the simulation, while the valve lift fell below 4 mm. When the valve lift was higher than 6 mm, the simulated swirl ratio gradually increased when the valve lift increased. Fig. 4 shows that the swirl ratio of most guide vane models cannot exceed that of the base model at a 4-mm valve lift.

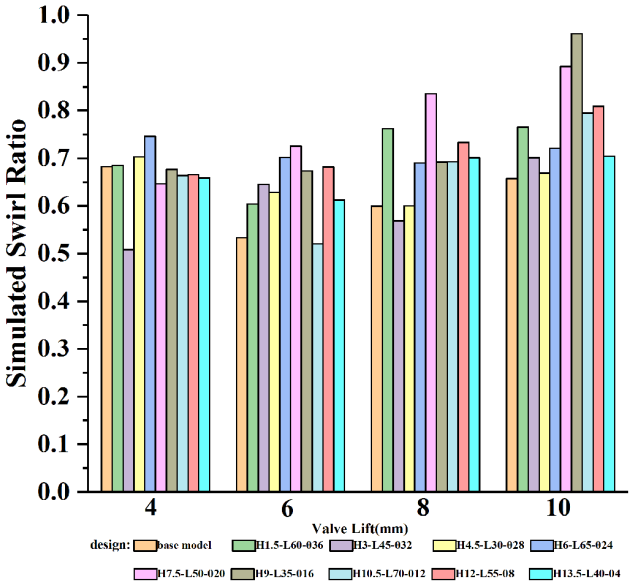

FIGURE 4. Simulated swirl ratio under different guide vane designs and valve lifts.

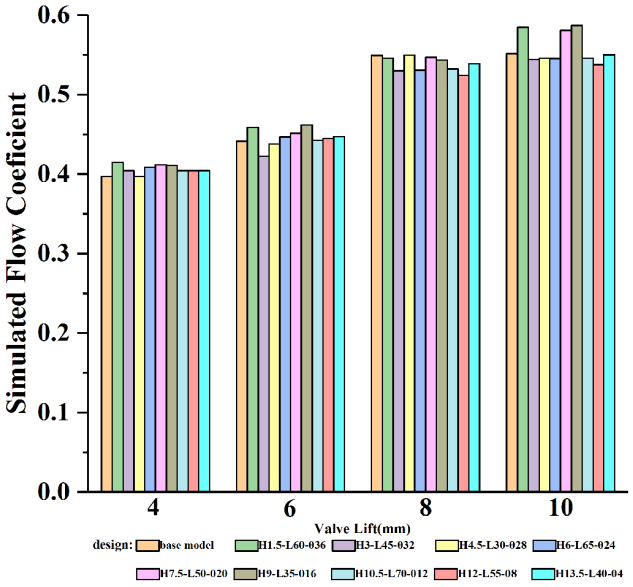

FIGURE 5. Simulated flow coefficient for different guide vane designs and valve lifts.

However, design 4 H6-L65-θ24 could obviously improve the swirl ratio compared to the base model at a 4-mm valve lift. When the valve lift exceeded 6 mm, most swirl ratios produced by different guide vane models were greater than that of the base model. Furthermore, design 5, H7.5-L50-θ20, had the highest swirl ratio with the 6-mm and 8-mm valve lifts and second best swirl ratio with the 10-mm valve lift. Design 6, H9-L35-θ16, had the highest swirl ratio with the 10-mm valve lift.

Fig. 5 shows the simulated flow coefficient for different guide vane designs and valve lifts. The flow coefficient

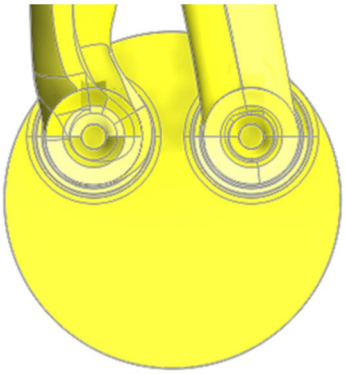

FIGURE 6. View location.

marginally changed. The guide vane models could not increase the flow coefficient over the base model, which lacked a guide vane. However, the flow coefficients of some guide models improved compared to that of the base model at some valve lifts. The flow coefficient of the guide vane models differed within 5% from that of the base model. Over a definite range, there is a linear relationship between swirl ratio and flow coefficient: if one parameter increases, the other decreases [40]. In this study, most guide vane models improved the swirl ratio compared to the base model and slightly affected the flow coefficient, which could be ignored. Therefore, the guide vanes produced a meaningful effect.

D. DYNAMIC CHARACTERISTICS OF THE IN-CYLINDER DURING THE INTAKE STOKE

The main objective of this study was to explore the effect of guide vanes on the performance of a twin-intake diesel engine during the intake stroke and determine the optimal design. The simulation results show that design 4 (H6-L65-θ24),

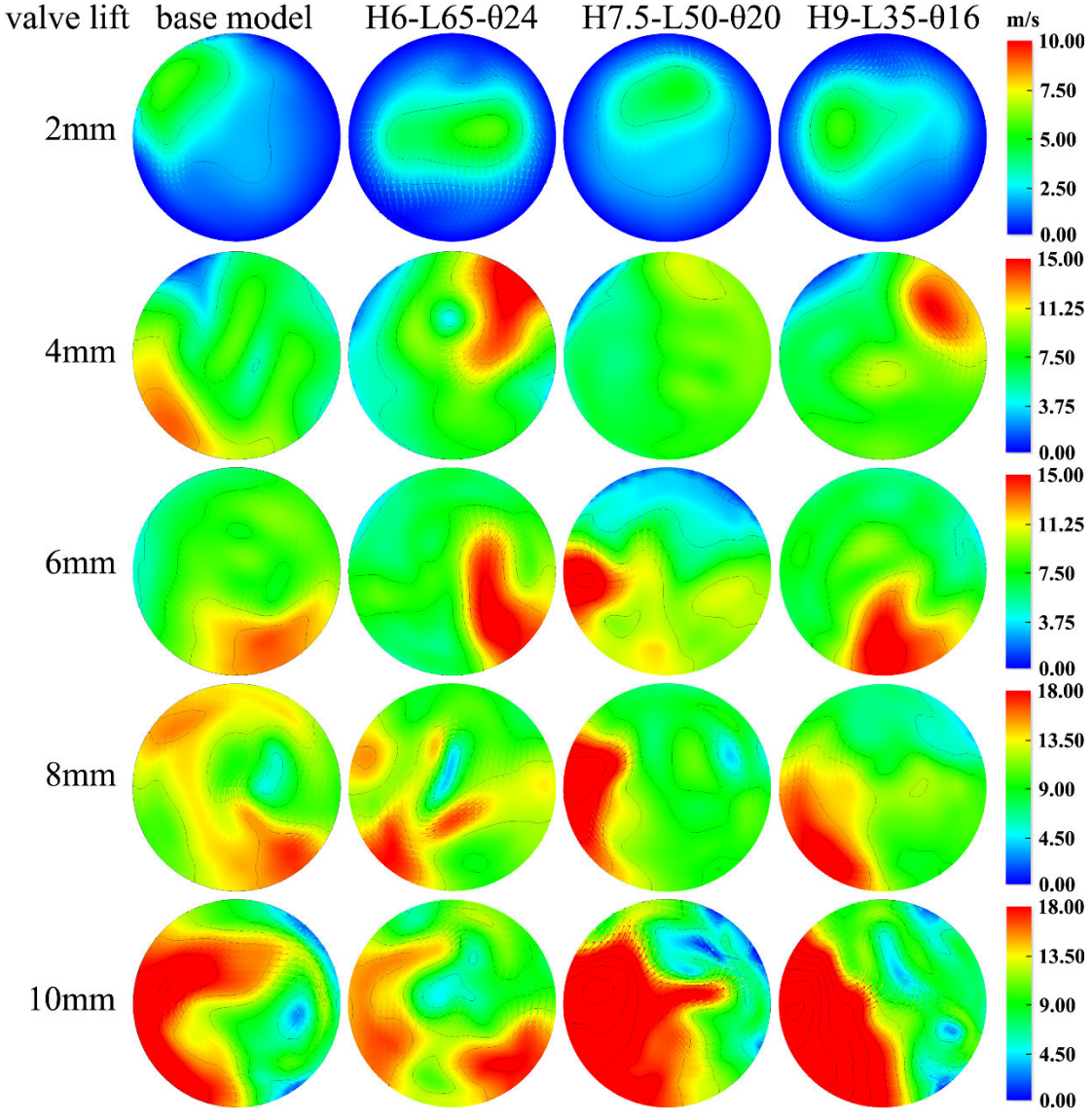

FIGURE 7. Flow velocity distribution for different designs and valve lifts.

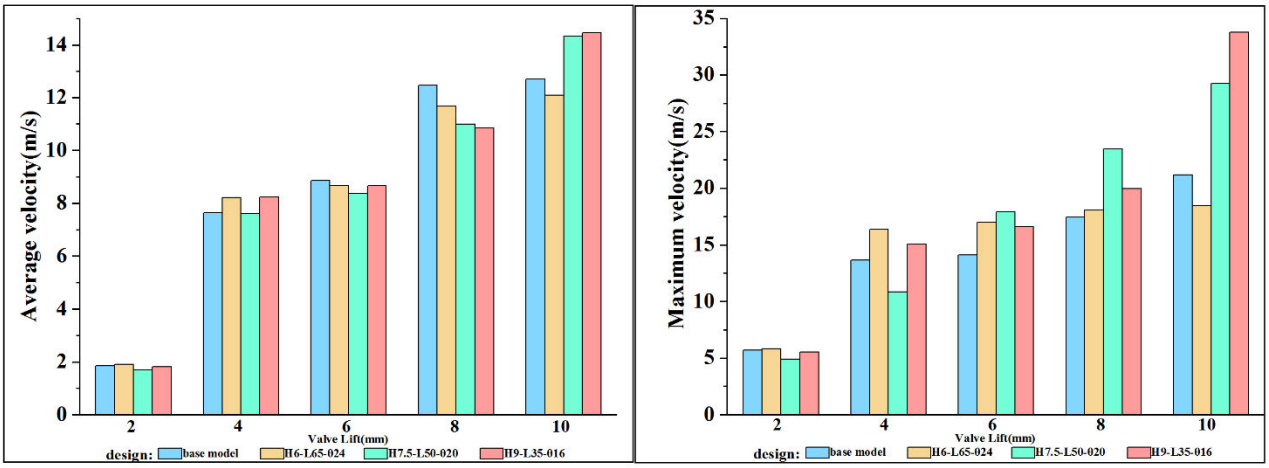

FIGURE 8. Comparison of the flow velocity for different designs and valve lifts.

design 5 (H7.5-L50-θ20) and design 6 (H9-L35-θ16) produced the most obvious improvements. Thus, this section further analyzes the flow field distribution of velocity and vorticity in the base model and optimized guide vane models. Fig. 6 shows the location of the transverse section to evaluate each physical quantity.

All transverse sections were viewed from the same position. The experimental flow characteristics were studied on a steady-flow bench with a vane anemometer at 1.75D. Therefore, the velocity and vorticity along the transverse section at 1.75D were selected for analysis. The dynamic characteristics of the in-cylinder during the intake stroke are shown in Figs. 7 and 9. Each column shows the physical quantity distribution under different valve lifts for the same designs, and each row represents the physical quantity distribution of different designs for the same valve lift. The flow field is colored according to the magnitude of the field on the cutting plane. The physical quantity vectors are visualized on a cutting plane. Details of the physical quantity vector field are represented by arrows; the arrow density and length can be customized. The isocontours are shown on the cutting plane.

For the velocity distribution, we pay attention to the location of the high-speed area and uniformity of the velocity distribution. From the flow velocity distribution for different designs and valve lifts in Fig. 7, the flow velocity increases with the increase in valve lift, and the high-speed distribution areas of different designs are different, so the guide vanes will affect the spatial distribution of the velocity in the cylinder. When the valve lift increases, an obvious high-speed concentrated area appears. Compared to the basic model, the high-speed area of the guide vane modes is relatively high and concentrated. When the valve lift increases, the flow field obviously rotates in a clockwise direction, and the regularity is stronger. Hence, the guide vane has a better effect on organizing air flow. The uniformity of the flow velocity distribution is poor when the valve lift is high. There are differences in different designs and valve lifts. At the 2-mm valve lift, the flow velocity hardly changes and is relatively uniform. When the valve lift is 4 mm and 6 mm, Design 4 (H6-L65-θ24) has more high-speed areas and a uniform flow rate. When the valve lift is 8 mm and 10 mm, the high-speed areas of design 5 (H7.5-L50-θ20) are redundant with other designs.

Furthermore, the average and maximum velocities increase when the valve lift increase, as shown in Fig. 8. The primary cause is that the valve seat decreases the resistance to flow when the valve lift increases. There is a throttle effect near the valve seat, and the throttle effect decreases as the valve lift increases. The guide vane also produces a throttle effect. The throttle effect is weakened at higher valve lifts. When the valve lift is 6 mm and 8 mm, the average velocity of the guide vane models cannot exceed that of the base model. However, the maximum velocities of the guide vane models are more focused and larger than that of the base model. Design 5 (H7.5-L50-θ20) and design 6 (H9-L35-θ16) had better average and maximum velocities at a 10-mm valve lift than at the other valve lifts. The guide vane affects the velocity distribution of the flow field and increases the high-speed area, which is conducive to the formation of a mixture.

The flow vorticity variations are shown in Fig. 9. The arrangement is similar to that in Fig. 7, except the physical variable of the field is the vorticity. As stated earlier, the vorticity is defined as the curl of the velocity vector, which is twice the angular velocity in units of s^{-1} (s is the time in seconds). Swirl is a type of structure form of the vorticity field. In diesel engines, a larger and more concentrated vorticity is more conducive to form its rapid rotational motion to organize the air movement in the cylinder well and improve the fuel-air mixing rate and combustion rate of the diesel engine. As shown in Fig. 9, the vorticity distribution follows a similar trend as the velocity distribution, which increases when the valve lift increases. When the valve lift is 2 mm, the vorticity distribution of the guide vane model is more uniform than the basic model and concentrated in the middle of the

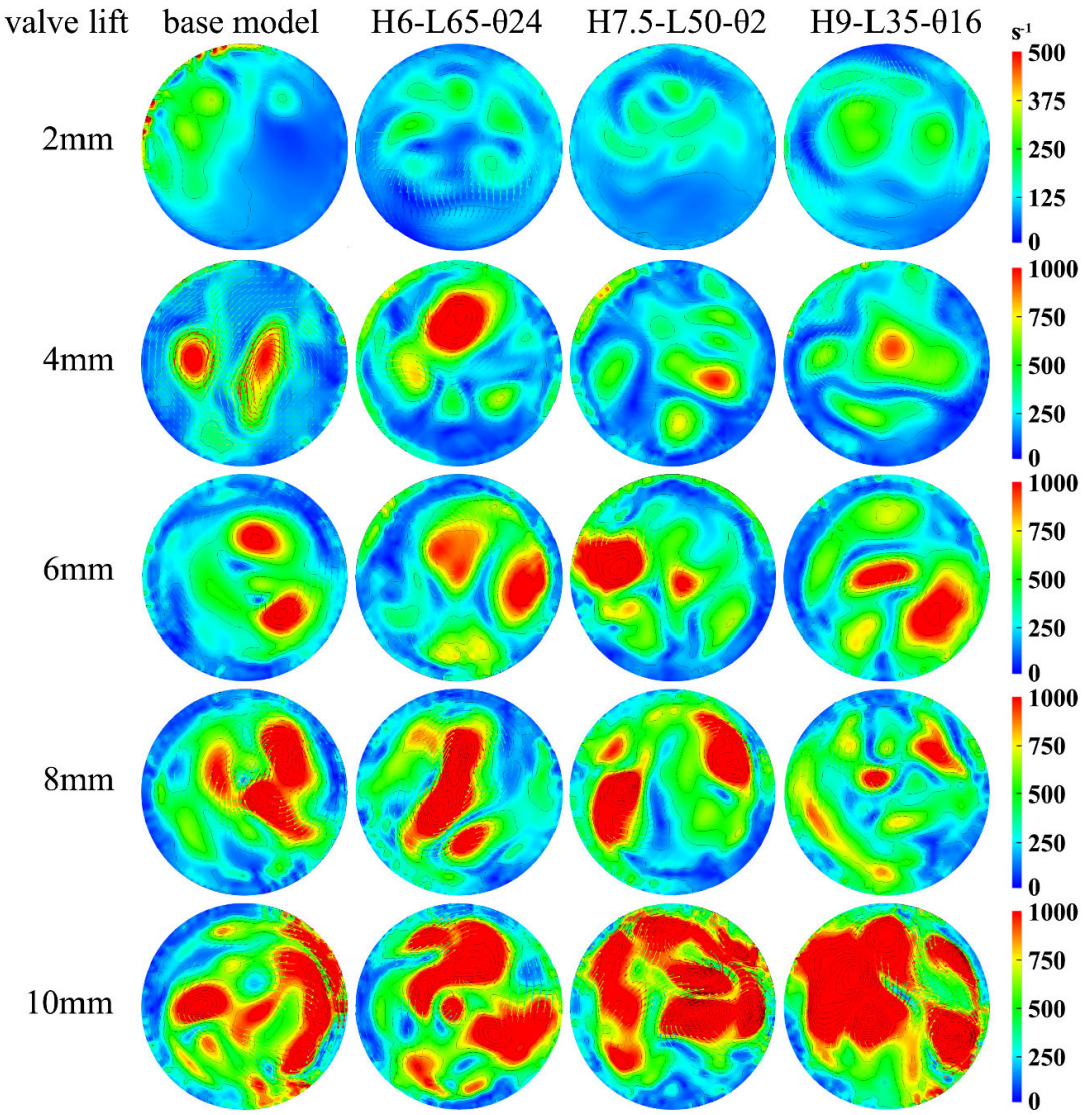

FIGURE 9. Flow vorticity distribution for different designs and valve lifts.

cylinder. When the valve lift increases, the vorticity of the guide vane model is more evenly distributed in the cylinder, especially when the valve lift is 10 mm, which is conducive to the formation of mixed gas, improves the combustion quality, increases the fuel efficiency and reduces pollutant emissions. As shown in Fig. 10, most of the guide model models have better average vorticities than the base model, except for the 2-mm valve lift. For the maximum vorticity, the improvement provided by design 4 (H6-L65-θ24) with the 4-mm valve lift is better than that of the other designs; above a 6-mm valve lift, design 5 (H7.5-L50-θ20) provides the best effect; at a 10-mm valve lift, design 6 (H9-L35-θ16) provides the best effect.

IV. EXPERIMENTS

A steady-flow bench test is considered an industry standard for these types of measurements [41]. The steady-flow test is a valuable method to evaluate the performance of engine intake ports [42]. At present, there are 4 main evaluation methods: AVL method, FEV method, Ricardo method and SwRI method [43]. Readers are encouraged to refer to more details on the above techniques in the literature [44], [45]. In this study, based on a practical structure of a twin-intake system for a diesel engine, a steady-flow bench was reasonably simplified and established. The performance of the twin-intake diesel engine was evaluated by the AVL method.

A. FABRICATION OF THE GUIDE VANES

Based on the simulation results, design 4 (H6-L65-θ24), design 5 (H7.5-L50-θ20) and design 6 (H9-L35-θ16) produced the best effects with different valve lifts. In the experiments, all simulation designs were validated to ensure a comprehensive study of the effect of guide vanes on the flow characteristics of diesel engines. Individual guide vanes were constructed with different heights and lengths according to Table 1, and the corresponding angles were adjusted when

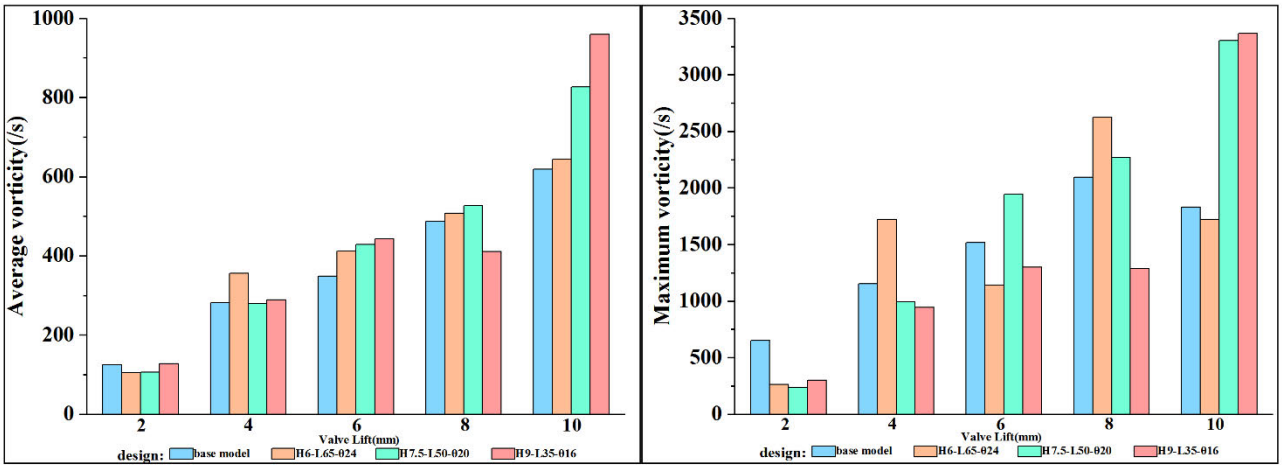

FIGURE 10. Comparison of the flow vorticity for different designs and valve lifts.

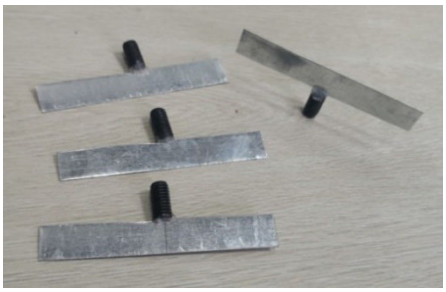

FIGURE 11. A set of guide vanes.

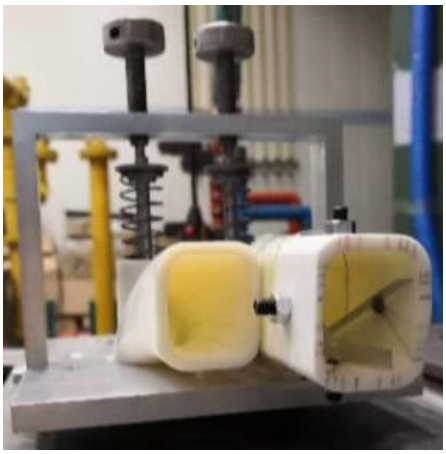

FIGURE 12. A guide vane installation in an experiment.

they were installed in front of the helical intake port. The section in front of the intake port was prepared by 3D printing according to the real dimensions. The fabricated guide vanes and their installation in the experiment are illustrated in Figs. 11 and 12.

B. EXPERIMENTAL SET-UP

The intake port was designed based on the swirl ratio and flow coefficient determined in the steady-flow test and was used to

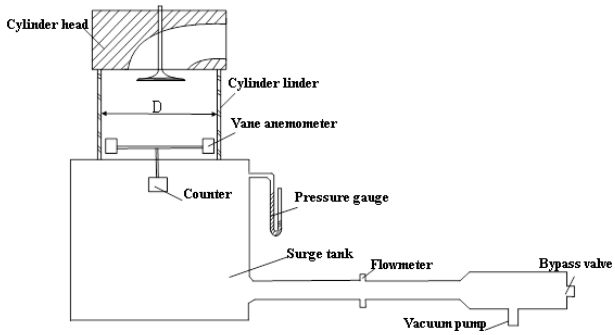

FIGURE 13. Schematic diagram of the steady-flow test bench.

evaluate the performance of the intake port. The schematic diagram of the steady-flow test bench is shown in Fig 13, which was mainly composed of a cylinder head, a cylinder liner, a vane anemometer, a counter, a pressure gauge, a surge tank, a flowmeter, a vacuum pump and a bypass valve. In this experiment, the vacuum pump maintained the pressure difference between the inside of the bench and the atmospheric pressure to a certain range. When air enters the cylinder through the guide vane along the intake port, an intake swirl is generated and makes the vane on the vane anemometer rotate. The rotational speed of the vane anemometer is counted by the counter. There are flowmeters and pressure gauges on the test bench to measure real-time parameters during the experiment.

The sensors are connected to the required test parts. After the equipment is started, the pressure and temperature generated inside the components are used to determine whether the indicators satisfy the requirements. Then, the measured parameters and results are recorded and displayed on the console. The operation range and uncertainties of the main components are shown in Table 4. During the test, the base model without a guide vane was run on the test bench first, and the performance was taken as the baseline. The valve lift was adjusted from 2 to 10 mm by adjusting the bolt, and the

TABLE 4. Operation range and uncertainties of the main components.

Components	Operation range	Uncertainties
Vane anemometer	1-9999 r/min	±15r/min
pressure gauge	0-14 kPa	±0.07 kPa
flowmeter	0-2720 m^3/h	±10 m3/h
vacuum pump	9.8-98 kPa	±4.9 kPa

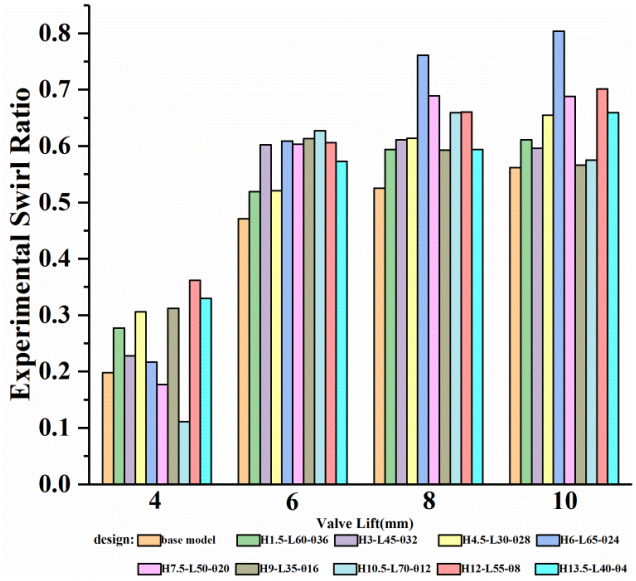

FIGURE 14. Experimental swirl ratio for different guide vane designs and valve lifts.

step was 2 mm. The console desk recorded the relevant data after each operation. Then, the 9 fabricated guide vanes were installed on the base model and individually tested according to the above procedure. Finally, the data were sorted, compared and analyzed. The detailed results are described in the following section.

C. EXPERIMENTAL RESULTS

Fig. 14 shows the experimental swirl ratio for different guide vane designs and valve lifts. Because of different flow patterns and mechanisms under different valve lifts [46], [47], the main flow state through the valve changes. When the valve lift is small, the airflow adheres to the surface of the valve. When the valve lift increases, the airflow gradually separates from the valve. We find that the diesel engine gas flow in this article can stably exist after the 4-mm valve lift. The swirl ratio greatly fluctuates below valve lifts of 2 and 4 mm, which is similar to the simulation results; the presented experimental results are for valve lifts of 4-10 mm with steps of 2 mm. Similarly, the experimental swirl ratio gradually increases when the valve lift increases. As shown in Fig. 14, all guide vane models have better experimental swirl ratios than the base model except at a valve lift of 4 mm. At 4-mm valve lift, most of the designs offer better performance

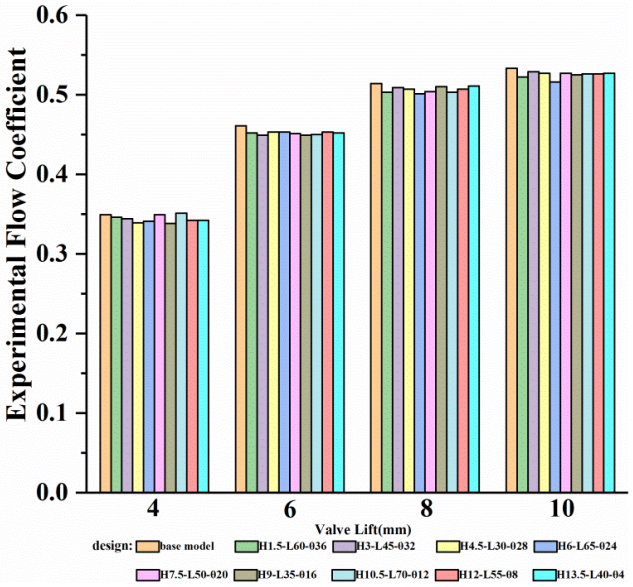

FIGURE 15. Experimental flow coefficient for different guide vane designs and valve lifts.

than the base model. Design 4 (H6-L65-θ24) offers the best performance improvement overall, especially at higher valve lifts. Design 5 (H7.5-L50-θ20) produces the second best experimental swirl ratio. The highest recorded experimental swirl ratio is achieved with design 4 (H6-L65-θ24) with a maximum improvement of approximately 45% at a 10-mm valve lift. These results show that the guide vane models have better experimental swirl ratio than the base model without a guide vane, especially at high valve lifts.

Fig. 15 shows the experimental flow coefficient for different guide vane designs and valve lifts. The flow coefficient increases when the valve lift increases primarily because the resistance loss gradually decreases with the valve lift. The analysis of the experimental flow coefficient for all designs reveals that none of the flow coefficients of the guide vane models was better than that of the base model primarily because the guide vane restricts the intake air flow. Compared to the base model, the flow coefficient of all guide vane models was slightly reduced. Thus, the guide vane acts as a slight barrier to the airflow. However, the maximum reduction in the experimental flow coefficient compared to the base model is approximately 3% and was obtained with design 4 (H6-L65-θ24) at a 10-mm valve lift. Hence, the guide vane slightly affects the flow coefficient of a twin-intake diesel engine, but this effect can be ignored.

V. COMPARISON OF THE SIMULATION AND EXPERIMENTAL RESULTS

Fig. 16 shows a comparison of the experimental and simulated swirl ratios for different designs and valve lifts. The experimental and simulation results are consistent. However, the simulated swirl ratio is slightly higher than the experimental one, especially at a low valve lift. The major cause of this difference is that the vane anemometer hinders the

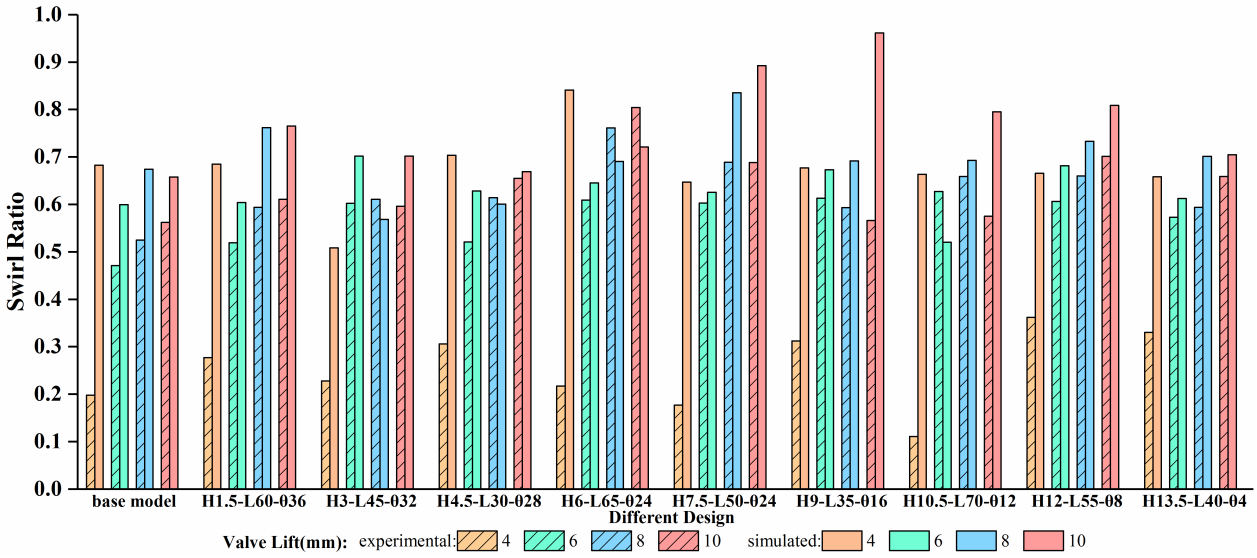

FIGURE 16. Comparison of the experimental and simulated swirl ratios.

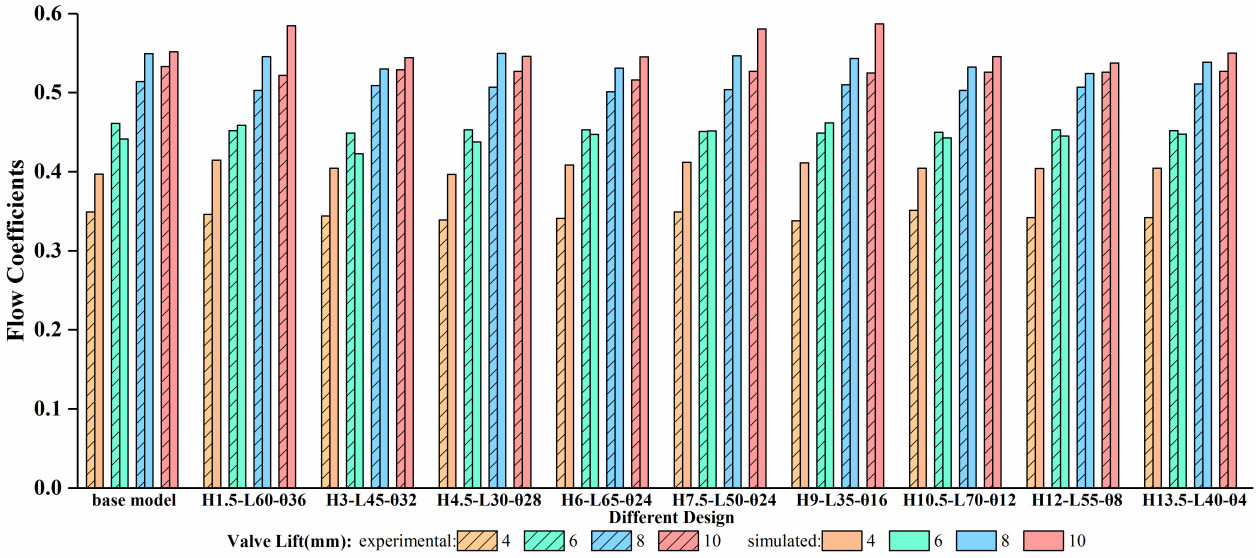

FIGURE 17. Comparison of the experimental and simulated flow coefficients.

airflow in the steady-flow test. As mentioned earlier, the fluid movement is different under different valve lifts, which have a greater impact at low valve lifts, but the simulation and test have good consistency at high valve lifts. Both experimental and simulated swirl ratios increase with increasing valve lifts, except in the simulation of a 4-mm valve lift. The maximum experimental and simulated swirl ratios were achieved with different designs. One of the reasons is that the simulation used a simulated speed instead of the actual speed, which produces errors. In addition, the uniform design determines the optimized design, which is not the optimal design, and the real optimal result may be somewhere between the two optimized designs.

Fig. 17 shows a comparison of the experimental and simulated flow coefficients with different designs and valve lifts. The experimental and simulated flow coefficients show similar trends and are consistent with each other. Both experimental and simulated flow coefficients increase when the valve lift increases. Moreover, the simulated flow coefficient is slightly higher than the experimental value, especially for the 4-mm valve lift, due to the same reason as for the above swirl ratio results. The vane anemometer hinders the airflow in the steady-flow test, and there is no vane anemometer in the simulation.

VI. CONCLUSION

In this research, we performed experiments and simulations to investigate the effect of guide vanes with different lengths, heights and angles, which were installed in front of a helical intake port, on the flow characteristics of a diesel engine with twin intake ports. The main conclusions of this article are presented below:

1. During the intake stroke, the flow coefficient increases when the valve lift increases. The guide vane appears to provide resistance to the airflow, and the flow coefficient of the guide vane models is slightly reduced by approximately 3% at most. The effect of the guide vane on the flow coefficient is negligible. The experimental and simulation results are consistent.

2. The swirl ratio increases when the valve lift increases, especially at a high valve lift. The guide vane models greatly affect the swirl ratio. Moreover, identical guide vane models with different valve lifts have different effects. The optimal guide vane models for different valve lifts are not the same.

3. Compared to the base model, the swirl ratio average increase of guide vane models is 21%. The maximum increase is 39% when the guide vane height is 6 mm, the length is 65 mm, and the angle is 24°; when the guide vane height 7.5 mm, length of 50 mm and angle of 20°, average increase followed by 27%. The average reduction rate of discharge coefficient is less than 2%.

4. The effect of the guide vane on the flow coefficient was small, but the influence on the swirl ratio was considerable. Considering the trade-off relationship between flow coefficient and swirl ratio, it can be considered that the guide vane model can promote the flow characteristics of the performance of a twin-intake diesel engine.

REFERENCES

[1] D.-J. Lim and D.-H. Yang, "Assessment of regulatory requirements on technological changes: The increasing dominance of downsized turbo/super-charged engines over naturally aspirated engines," *IEEE Access*, vol. 7, pp. 84839–84848, 2019, doi: 10.1109/ACCESS.2019.2924665.

[2] S. Pischinger, "Current and future challenges for automotive catalysis: Engine technology trends and their impact," *Topics Catal.*, vol. 59, nos. 10–12, pp. 834–844, Jul. 2016, doi: 10.1007/s11244-016-0557-3.

[3] H.-L. Kui, H.-Z. Wang, W.-X. Ni, Y.-F. Chen, and J. Li, "Flow characteristics in diesel helical intake port bionic with non-smooth surface," *Jilin Daxue Xuebao Gongxueban, J. Jilin Univ. Eng. Technol. Ed.*, vol. 44, no. 3, pp. 668–674, 2014, doi: 10.13229/j.cnki.jdxbgxb201403014.

[4] Y. Zhang, T. Chen, W. Zhuge, S. Zhang, and J. Xu, "An integrated turbocharger design approach to improve engine performance," *Sci. China E, Technol. Sci.*, vol. 53, no. 1, pp. 69–74, Jan. 2010, doi: 10.1007/s11431-009-0421-9.

[5] M. Auriemma, G. Caputo, F. E. Corcione, G. Valentino, and G. Riganti, "Fluid-dynamic analysis of the intake system for a HDDI diesel engine by STAR-CD code and LDA technique," *SAE Tech. Pap.*, vol. 112, no. 3, pp. 21–28, 2003, doi: 10.4271/2003-01-0002.

[6] S. A. Basha and K. R. Gopal, "In-cylinder fluid flow, turbulence and spray models—A review," *Renew. Sustain. Energy Rev.*, vol. 13, nos. 6–7, pp. 1620–1627, Aug. 2009, doi: 10.1016/j.rser.2008.09.023.

[7] G. Wang, W. Yu, X. Li, Y. Su, R. Yang, and W. Wu, "Study on dynamic characteristics of intake system and combustion of controllable intake swirl diesel engine," *Energy*, vol. 180, pp. 1008–1018, Aug. 2019, doi: 10.1016/j.energy.2019.05.162.

[8] G. Wang, W. Yu, X. Li, Y. Su, R. Yang, and W. Wu, "Experimental and numerical study on the influence of intake swirl on fuel spray and in-cylinder combustion characteristics on large bore diesel engine," *Fuel*, vol. 237, pp. 209–221, Feb. 2019, doi: 10.1016/j.fuel.2018.09.156.

[9] W. Du and X.-R. Li, "Effect of guiding vanes in swirlers for use on diesel engines on the air flow," *Beijing Ligong Daxue Xuebao, Trans. Beijing Inst. Technol.*, vol. 24, no. 10, pp. 854–857, 2004, doi: 10.15918/j.tbit1001-0645.2004.10.003.

[10] X. Xin, D. X. Liu, L. Q. Wang, and L. Wang, "Influence of variable swirl intake manifolds for DI diesel engine on in-cylinder air motion," *Appl. Mech. Mater.*, vols. 130–134, pp. 95–98, Oct. 2011, doi: 10.4028/www.scientific.net/AMM.130-134.95.

[11] S. Bari and I. Saad, "Improvements of performance and emissions of a diesel-gen-set with biodiesel having guide vanes of various angles," in *Proc. Int. Mech. Eng. Congr. Expo.*, 2016, Art. no. V06AT08A005, doi: 10.1115/imece2016-65994.

[12] S. Bari and I. Saad, "Performance and emissions of a compression ignition (CI) engine run with biodiesel using guide vanes at varied vane angles," *Fuel*, vol. 143, pp. 217–228, Mar. 2015, doi: 10.1016/j.fuel.2014.11.050.

[13] S. Bari and I. Saad, "Simulation and experimental investigation of guide vane length to improve the performance of a diesel engine run with biodiesel," *J. Eng. Gas Turbines Power*, vol. 138, no. 11, pp. 1–13, Nov. 2016, doi: 10.1115/1.4033509.

[14] S. Bari and I. Saad, "Effect of guide vane height on the performance and emissions of a compression ignition (CI) engine run with biodiesel through simulation and experiment," *Appl. Energy*, vol. 136, pp. 431–444, Dec. 2014, doi: 10.1016/j.apenergy.2014.09.051.

[15] S. Bari and I. Saad, "CFD modelling of the effect of guide vane swirl and tumble device to generate better in-cylinder air flow in a CI engine fuelled by biodiesel," *Comput. Fluids*, vol. 84, pp. 262–269, Sep. 2013, doi: 10.1016/j.compfluid.2013.06.011.

[16] S. Bari and I. Saad, "Optimization of vane numbers through simulation and experiment, and investigation of the effect on the performance and emissions of a CI (compression ignition) engine run with biodiesel," *Energy*, vol. 79, pp. 248–263, Jan. 2015, doi: 10.1016/j.energy.2014.11.011.

[17] S. Bari and I. Saad, "Experimental investigation of adding vanes into the air intake runner of a diesel engine run on biodiesel to improve the air-fuel mixing," in *Proc. ASME Int. Mech. Eng. Congr. Expo.*, vol. 57434, Nov. 2015, Art. no. V06AT07A004, doi: 10.1115/IMECE2015-51900.

[18] S. Bari, P. J. G. Johansen, and A. J. T. Alherz, "Simulation of improvements to in-cylinder mixing of biodiesel with air by incorporating guide vanes into the air intake system," *Procedia Eng.*, vol. 105, pp. 480–487, 2015, doi: 10.1016/j.proeng.2015.05.079.

[19] D. W. Jia and X. W. Deng, "Intake flow interference analysis of combination intake port in diesel engine," *J. Appl. Fluid Mech.*, vol. 12, no. 1, pp. 61–67, Jan. 2019, doi: 10.29252/JAFM.75.253.29175.

[20] X. Liu, H. J. Yan, N. Tian, and G. Zhao, "CFD simulation analysis and research based on engine air intake system of automotive," in *Proc. 7th Int. Conf. Electron. Inf. Eng.*, vol. 10322, 2017, Art. no. 103224G, doi: 10.1117/12.2266425.

[21] H. Kim, S. Y. Lee, H. J. Kim, and J. T. Chung, "Numerical study on the effects of tumble and swirl on combustion and emission characteristics of an LPG direct injection engine," *Int. J. Automot. Technol.*, vol. 21, no. 3, pp. 623–632, Jun. 2020, doi: 10.1007/s12239-020-0059-y.

[22] Y. Wang and Y.-W. Leung, "Multiobjective programming using uniform design and genetic algorithm," *IEEE Trans. Syst., Man Cybern. C, Appl. Rev.*, vol. 30, no. 3, pp. 293–304, Aug. 2000, doi: 10.1109/5326.885111.

[23] J. Zhang, J. Feng, Y. Yang, and J.-H. Wang, "Finding community modules for brain networks combined uniform design with fruit fly optimization algorithm," *Interdiscipl. Sci., Comput. Life Sci.*, vol. 12, no. 2, pp. 178–192, Jun. 2020, doi: 10.1007/s12539-020-00371-x.

[24] J. Zhang, L. Tang, B. Liao, X. Zhu, and F. X. Wu, "Finding community modules of brain networks based on PSO with uniform design," *Biomed Res. Int.*, vol. 2019, pp. 33297–33317, Nov. 2019, doi: 10.1155/2019/4979582.

[25] J.-T. Tsai, P.-Y. Yang, and J.-H. Chou, "Data-driven approach to using uniform experimental design to optimize system compensation parameters for an auto-alignment machine," *IEEE Access*, vol. 6, pp. 40365–40378, 2018, doi: 10.1109/ACCESS.2018.2856911.

[26] H. Lu, X. Zheng, and Q. Li, "A combinatorial optimization design method applied to S-shaped compressor transition duct design," *Proc. Inst. Mech. Eng. G, J. Aerosp. Eng.*, vol. 228, no. 10, pp. 1749–1758, Aug. 2014, doi: 10.1177/0954410014531922.

[27] W.-Y. He, J.-H. Zhang, and J. Wang, "A comprehensive evaluation method of diesel engine sound quality based on paired comparison, uniform design sampling, and improved analytic hierarchy process," *J. Zhejiang Univ.-Sci. A*, vol. 18, no. 7, pp. 531–544, Jul. 2017, doi: 10.1631/jzus.A1600025.

[28] C. Ma and K.-T. Fang, "A new approach to construction of nearly uniform designs," *Int. J. Mater. Prod. Technol.*, vol. 20, nos. 1–3, pp. 115–126, 2003, doi: 10.1504/IJMPT.2004.003916.

[29] K.-T. Fang, M.-Q. Liu, H. Qin, and Y.-D. Zhou, "Construction of uniform designs—Deterministic methods," in *Theory and Application of Uniform Experimental Designs*. Singapore: Springer, 2018, pp. 101–154.

[30] P. Winker and K.-T. Fang, "Application of threshold-accepting to the evaluation of the discrepancy of a set of points," *SIAM J. Numer. Anal.*, vol. 34, no. 5, pp. 2028–2042, Oct. 1997, doi: 10.1137/S0036142995286076.

[31] D. W. Jia, X. W. Deng, and J. L. Lei, "Steady-state experiment and simulation of intake ports in a four-valve direct injection diesel engine," *J. Appl. Fluid Mech.*, vol. 11, no. 1, pp. 217–224, Jan. 2018, doi: 10.29252/jafm.11.01.27494.
[32] Z.-G. Feng and E. E. Michaelides, "The immersed boundary-lattice Boltzmann method for solving fluid–particles interaction problems," *J. Comput. Phys.*, vol. 195, no. 2, pp. 602–628, Apr. 2004, doi: 10.1016/j.jcp.2003.10.013.
[33] Z. G. Feng and E. E. Michaelides, "Hydrodynamic force on spheres in cylindrical and prismatic enclosures," *Int. J. Multiph. Flow*, vol. 28, no. 3, pp. 479–496, 2002, doi: 10.1016/S0301-9322(01)00070-2.
[34] R. Stoll, J. A. Gibbs, S. T. Salesky, W. Anderson, and M. Calaf, "Large-eddy simulation of the atmospheric boundary layer," *Boundary-Layer Meteorol.*, vol. 177, nos. 2–3, pp. 541–581, Dec. 2020, doi: 10.1007/s10546-020-00556-3.
[35] M. Abkar, H. J. Bae, and P. Moin, "Minimum-dissipation scalar transport model for large-eddy simulation of turbulent flows," *Phys. Rev. Fluids*, vol. 1, no. 4, pp. 1–10, Aug. 2016, doi: 10.1103/PhysRevFluids.1.041701.
[36] H. Kui, Y. Guo, P. Cheng, C. Fu, X. Liu, and G. Li, "Research on the flow characteristics of diesel engine with helical intake port based on XFlow," in *Proc. CICTP*, Nanjing, China, Jul. 2019, pp. 4097–4106.
[37] G. J. Micklow and W.-D. Gong, "Intake and in-cylinder flowfield modelling of a four-valve diesel engine," *Proc. Inst. Mech. Eng. D, J. Automobile Eng.*, vol. 221, no. 11, pp. 1425–1440, Nov. 2007, doi: 10.1243/09544070JAUTO504.
[38] Y.-Q. Wang, Y.-S. Gao, J.-M. Liu, and C. Liu, "Explicit formula for the Liutex vector and physical meaning of vorticity based on the Liutex-Shear decomposition," *J. Hydrodynamics*, vol. 31, no. 3, pp. 464–474, Jun. 2019, doi: 10.1007/s42241-019-0032-2.
[39] D. Szpica, "Determination of low pressure gas injector valve flow factor," *Eng. Rural Dev.*, vol. 2020, pp. 721–729, May 2020, doi: 10.22616/ERDev.2020.19.TF167.
[40] F.-S. Liu, W. Du, and X.-R. Li, "Matching of variable swirl intake port in double-intake-port diesel engine," *Beijing Ligong Daxue Xuebao, Trans. Beijing Inst. Technol.*, vol. 26, no. 9, pp. 789–792, 2006, doi: 10.15918/j.tbit1001-0645.2006.09.010.
[41] J. Fernández, E. J. Vega, A. Castilla, A. Marcos, J. M. Montanero, and R. Barrio, "An experimental setup for the study of the steady air flow in a diesel engine chamber," in *Proc. EPJ Web Conf.*, vol. 25, 2012, pp. 1–4, doi: 10.1051/epjconf/20122501014.
[42] M.-Q. Lin and W. Peng, "Steady flow test and numerical simulation of a GDI engine," in *Proc. 2nd Int. Conf. Electron. Mech. Eng. Inf. Technol. (EMEIT)*, 2012, pp. 1851–1854, doi: 10.2991/emeit.2012.410.
[43] Z.-W. Zhao, S.-L. Liu, D.-X. Liu, J.-C. Yu, and H.-Q. Feng, "Study on the test technology of steady state flow of port with variable pressure drop," *Neiranji Xuebao, Trans. CSICE, Chin. Soc. Intern. Combust. Engines*, vol. 22, no. 1, pp. 79–85, 2004, doi: 10.16236/j.cnki.nrjxb.2004.01.013.
[44] S. Jiang, S. Zhu, H. Wen, and S. Huang, "Parameter analysis of diesel helical intake port numerical design," *Energy Procedia*, vol. 16, pp. 558–563, Jan. 2012, doi: 10.1016/j.egypro.2012.01.090.
[45] F. Claudio, C. Cristian, C. Giulio, B. G. Marco, F. Stefania, B. Federico, V. Alessandro, and S. Stefano, "Numerical evaluation of the applicability of steady test bench swirl ratios to diesel engine dynamic conditions," *Energy Procedia*, vol. 81, pp. 732–741, Dec. 2015, doi: 10.1016/j.egypro.2015.12.079.
[46] D. Szpica, "Review of experimental methods of investigation of inlet system of piston combustion engine," *Przeglad Mechaniczny*, vol. 2, pp. 26–33, Jan. 2010.
[47] K. Tanaka, "Air flow through suction valve of conical seat part I. Experimental research," *Rep. Aeronaut. Res. Inst. Tokyo Imperial Univ.*, vol. 4, pp. 259–360 and Pl.13–Pl.16, 1929.

HAILIN KUI received the B.S. degree from the Dalian University of Technology, in 1990, and the M.S. degree in vehicle engineering and the Ph.D. degree from the Department of Vehicle Operation Engineering, Jilin University, Changchun, China, in 1999 and 2007, respectively.

He is currently a Professor with the College of Traffic and Transportation, Jilin University. His research interests include economy of vehicle energy saving, intelligent traffic control, vehicle road coordination, and others.

YUNZHEN GUO received the B.S. degree in traffic and transportation from the Shandong University of Technology, Zibo, China, in 2016. She is currently pursuing the Ph.D. degree with the Department of Vehicle Operation Engineering, Transportation College, Jilin University, Changchun, China.

Her research interests include economy of vehicle energy saving, and reducing drag and increasing vortex of diesel engine.

CHANGRAN FU received the B.S. degree in traffic and transportation from Jilin Agricultural University, Changchun, China, in 2016, and the M.S. degree in vehicle application engineering from Jilin University, Changchun.

His main research interest includes comprehensive energy-saving technologies for vehicles.

SHENGWEI PENG received the B.S. degree in vehicle engineering from Liaocheng University, Liaocheng, China, in 2017. He is currently pursuing the master's degree in vehicle application engineering with Jilin University.

His current research interests include automobile energy conservation and emission reduction.